



An enhanced constitutive model for quasi-brittle rocks with localized damage

Susheng Wang¹ · Lunyang Zhao² · Wanlu Zhang³

Received: 3 September 2021 / Accepted: 5 August 2022 / Published online: 9 September 2022
© The Author(s), under exclusive licence to Springer-Verlag GmbH Germany, part of Springer Nature 2022

Abstract

Localized deformation is the failure precursor of quasi-brittle rocks. The objective herein is to propose an enhanced constitutive model incorporating the evolution of localized damage in quasi-brittle rocks. The plastic and damage behaviors are assumed inside the localization zone, and elastic deformation is considered outside the zone. As a consequence, the macroscopic responses are obtained by using a volume average procedure incorporating the evolution of the volume fraction of the localization zone. The plastic and damage behaviors inside the localization zone are, respectively, described by a nonlinear yield criterion and an exponential damage criterion. The onset of localized failure is defined by introducing a critical value of localized damage parameter. For application, a semi-implicit return mapping algorithm is developed to deal with the numerical implementation at the material level. Finally, the validity of the model and the robustness of the algorithm are assessed by the consistent comparison between simulation results and the triaxial compression test of three typical quasi-brittle rocks. The post-peak snapback and brittle-ductile transition behaviors are captured by adjusting the evolution rates of localization zone and localized damage, respectively. This model has two main innovative features: (1) the simulated peak strength of the model only depends on the strength parameters and is not affected by the damage and localization parameters, and (2) the proposed approach can effectively overcome the over-estimation of plastic deformation by the traditional associated plastic flow rule and accurately describe the post-peak mechanical behaviors of quasi-brittle rocks.

Keywords Associated plastic flow · Constitutive model · Damage evolution · Localization effects · Quasi-brittle rocks

List of symbols

[**u**] Local displacement jump
n Normal vector

h Width of the band
H Height of the sample
 ξ Volume fraction of the band
 Σ Macroscopic stress tensor
E Macroscopic strain tensor
 σ_i Stress tensor inside the band
 σ_o Stress tensor outside the band
 ε_o Local elastic strain tensor
 ε_i^d Local damage strain tensor
 ε_i^e Recoverable strain
 ε_i^p Local irreversible plastic strain tensor
 \mathbb{C}_o Fourth-order elastic stiffness tensor
 $\mathbb{C}(\omega)$ Fourth-order damage stiffness tensor
f_p Plastic yield function
f_d Damage function
G Plastic potential function
 $\alpha(\omega)$ Plastic hardening/softening function
 η Strength parameter
m Strength parameter
C_o Strength parameter

✉ Lunyang Zhao
zhao_l_y@foxmail.com

- ¹ State Key Laboratory for Geomechanics and Deep Underground Engineering, School of Mechanics and Civil Engineering, China University of Mining and Technology, Xuzhou 221116, China
- ² South China Research Institute On Geotechnical Engineering, School of Civil Engineering and Transportation, South China University of Technology, Guangzhou 510641, China
- ³ National-Regional Joint Engineering Research Center for Soil Pollution Control and Remediation in South China, Guangdong Key Laboratory of Integrated Agro-Environmental Pollution Control and Management, Guangdong Engineering Research Center for Non-Point Source Pollution Control, Institute of Eco-Environmental and Soil Sciences, Guangdong Academy of Sciences, Guangzhou 510650, China

ω_c	Damage parameter
ω_{cr}	Critical damage
ω_{max}	Maximum damage value
Y_o	Damage-driven force threshold
λ_p	Plastic multiplier
λ_d	Damage multiplier
Y_d	Damage-driven force
ζ	Parameter controlling local bandwidth evolution
ω	Damage variable
σ_i^{trial}	Trial stress tensor
ε_i^{trial}	Trial strain tensor
k	Loading step
d	Increment between loading steps
δ	Tiny increment between iteration steps
φ	Friction angle
θ_c	Failure angle

1 Introduction

Due to the high in-situ stress conditions, the mechanical behaviors of quasi-brittle rocks (such as granite [8], sandstone [32], and basalt [19], etc.) play a dominant role in the deep underground engineering. Localized deformation or damage is the main failure mode of the hard or quasi-brittle rocks [13]. Localized cracks or shear/compression bands are often observed in failure rock samples and need special remedy in the numerical simulation [3, 12, 27]. The simulation and description of the localization failure mechanisms of rocks are prerequisite for the instability and failure analysis of practical engineering structure. The objective of this paper is to develop a characterization method that links the localized responses to the global mechanical behavior and propose a localized damage model to capture the mechanical responses of quasi-brittle rocks.

In the process of rock deformation and failure, the nonlinear characteristics are obvious, such as confining pressure effect, straining hardening/softening, volumetric dilatancy, stiffness degradation, brittle-ductile transition, anisotropy, and time-dependent behaviors, etc. [4, 29, 33, 37, 39]. These mechanical characteristics are related to mineral compositions [11], loading conditions [46], stress path [30, 41], and external environmental conditions [6, 26], etc. For quasi-brittle rocks, localized failure is an important characteristic accompanied by post-peak stress drop even under the high confining pressure [28]. Due to the influence of rock lithology and instrument stiffness, two typical failures (Class I and Class II) appear under compression condition [36]. The failure characteristics of Class I rock are as follows: deformation continues to increase during post-peak softening stage, while strain

decreases with decreasing of stress (snapback) after peak strength for Class II rock. These post-peak mechanical behaviors of quasi-brittle rocks are captured by the circumferential or minimum principal strain-controlled way in the laboratory [28]. In addition, the brittle-ductile transition behavior may occur with increasing of confining pressure [29]. This mechanical phenomenon can be briefly summarized that rock sample exhibits brittle failure with a rapid stress drop at the post-peak stage under low confining pressure while ductile deformation is almost without reduction carrying capacity at the post-peak stage under high confining pressure.

The physical failure mechanisms of quasi-brittle rocks can be interpreted by cracks initiation, propagation, and coalescence in localization zone. The corresponding nonlinear behaviors can be attributed to the damage accumulation induced by cracks propagation and the plastic deformation caused by frictional slipping between crack surfaces [2, 7]. Moreover, the coupling process of plastic and damage dissipation is the resource of nonlinear deformation of quasi-brittle rocks. Extensive works have been studied experimentally and theoretically on investigating localized deformation. This process of quasi-brittle rocks was well detected using advanced techniques, such as digital image correlation (DIC), computed tomography (CT), and acoustic emission (AE). At present, DIC [14] on localized strain field of rocks is mainly focused on uniaxial compression tests. The onset and propagation of localization band was tracked as well as its thickness and direction measured by CT [1]. The localized damage under the confining pressure was explored by AE [20] and CT [40]. Unfortunately, most of the existing research results are qualitative description and lack of a strong quantitative validation. Moreover, the localized quantitative experimental studies focus on the local strain field, and the local stress field information is difficult to obtain.

Rock constitutive model is acknowledged as an effective and essential approach to understand the nonlinear mechanical responses of rocks. The continuum damage mechanics (CDM) is a powerful theory tool to describe the mechanical behaviors of rocks. Based on the failure mechanism analysis of rocks, one or more internal variables are needed to characterize the relevant nonlinear dissipation process. For example, a coupled elastoplastic damage model [33] is proposed and developed for describing the two dissipation processes (plastic slipping and damage evolution). Because the associated flow rule tends to overestimate the nonlinear deformation of geomaterials, a non-associated flow rule is inevitably adopted in the model [42]. Moreover, the existing models describe the nonlinear and post-peak mechanical behaviors by changing the form of yield surface or incorporating an empirical function in the yield criterion [31, 44] without

considering localization effects. This causes the classical continuum models, which define homogeneous macroscopic variables over the volume element, are disabled to describe the localized failure characteristics, especially for post-peak localization behaviors.

In order to capture the localization deformation and failure characteristics as well as cracks propagation of quasi-brittle rocks, the existing methods are mainly divided into two categories. The first one is localized constitutive model [9, 18, 23], which were developed incorporating localized characteristics through regularization method at the material scale. The second class includes the improvement of the traditional numerical method and the innovation of advanced numerical method combining with a simple model used to capture the local cracks propagation of quasi-brittle rocks [16, 21, 45]. This work will study the localized failure of quasi-brittle rocks falling into the first category. For this purpose, enrichment of constitutive kinematics and embedded discontinuity has been applied separately to construct the constitutive model at the Gauss point and element level [5, 18]. The onset and orientation of localization band are the key points in the strain localization theory. Bifurcation theory is the landmark method to detect the onset and orientation of localized failure [22]. Mohr's maximization postulate has also been determined the direction of the cracks by finding the maximum value of yield function [34, 43]. So far, the loss of positive definiteness of the acoustic tensor [23] and the extremum of yield [9] have been widely used and successfully predicted the onset of the localization band. The nonlinear energy dissipation process occurs inside localized cracks after localization. In order to capture the localization responses, the mechanical responses of localized cracks are described by a specific traction-based friction-damage model [43]. How to develop localized damage models based on the CDM theory is still an open issue. Therefore, the main task of this study is to develop a rock constitutive model considering localized damage based on the general agreement of failure mechanism of quasi-brittle rocks.

The structure of the paper is as follows. The enrichment strain field, which is used to characterize the local discontinuous behavior, is presented in Sect. 2. Constitutive formulations are given in Sect. 3. Subsequently, the numerical implementation procedure is derived in detail in Sect. 4. And the model parameters identification, numerical validation, and numerical algorithm assessment are presented in Sect. 5. Finally, conclusions and prospects are drawn in Sect. 6. It is noted that the compression stress is assumed positive and tensile stress is assumed negative in this work.

2 Localization fundamentals

The localized failure is a remarkable characteristic of quasi-brittle rocks. This failure process translates from diffuse/homogeneous deformation to localized/inhomogeneous deformation due to the initiation, propagation, and macrocracks coalescence of cracks (in Fig. 1). A local shear band is the prominent compression-shear failure mode of quasi-brittle rocks. This causes the strong localized discontinuity behavior and localized damage to take place. Moreover, the nonlinear mechanical behaviors are governed by the local responses in the shear band. This section introduces a double-scale method that connect the macroscopic volume-averaged responses with mechanical responses inside and outside localization zone.

The damage failure process of quasi-brittle rocks is characterized by a local band embedded in the element once localization occurs (in Fig. 2). Moreover, the variation of bandwidth is also considered varying with the localized damage in the following work. The assumptions of traditional continuum model are not valid due to the embedded localization band in the volume element. Inspired by the previous studies [17], the local displacement jump $[\mathbf{u}]$, normal vector \mathbf{n} , and additional strain $\frac{1}{h}([\mathbf{u}] \otimes \mathbf{n})^{\text{sym}}$ are in the localization of the damage zone. The width of the band is h and the height of the sample is H . Assume that the sample is unit thickness. The volume fraction of the localization band can be defined by $\xi = h/H$. The macroscopic strain tensor \mathbf{E} over the total domain is calculated by the volume averages of strains inside and outside the band.

$$\mathbf{E} = \xi \mathbf{\varepsilon}_i + (1 - \xi) \mathbf{\varepsilon}_o \quad (1)$$

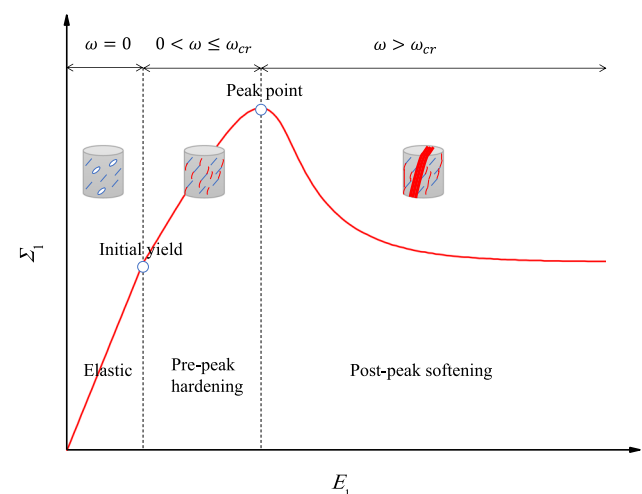


Fig. 1 Schematic illustration of localized cracks growth and propagation

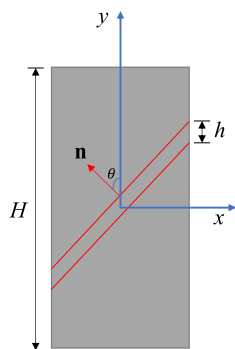


Fig. 2 Illustration of localization band with the normal vector \mathbf{n} in two-dimensional plane

where ε_o and ε_i represent strains inside and outside the band, respectively.

It is assumed that the nonlinear dissipation process is only considered inside the band and elastic unloading is outside the band. In view of the localized damage effect, ε_i consists of a recoverable strain ε_i^e and an irreversible plastic strain $\varepsilon_i^p = \frac{1}{h}([\mathbf{u}] \otimes \mathbf{n})^{sym}$. ε_i^e can be further decomposed by an elastic strain ε_o and a damage strain ε_i^d . Therefore, the macroscopic strain increment $d\mathbf{E}$ can be further written as follows

$$d\mathbf{E} = d\varepsilon_o + \xi d\varepsilon_i^d + \frac{\xi}{h}([\mathbf{du}] \otimes \mathbf{n})^{sym} \tag{2}$$

Supposed that the mechanical responses of the hierarchical structure can be reflected by the CDM theory. As the above-mentioned assumption, the generalized Hook’s law is used to describe the elastic response outside the band, while the elastoplastic damage theory is used to describe the nonlinear response inside the band. The constitutive relations outside and inside band are, respectively, given as the following formulations.

$$\boldsymbol{\sigma}_o = \mathbb{C}_o : \boldsymbol{\varepsilon}_o, \boldsymbol{\sigma}_i = \mathbb{C}(\omega) : \boldsymbol{\varepsilon}_i^e \tag{3}$$

where \mathbb{C}_o is the fourth-order elastic stiffness tensor and $\mathbb{C}(\omega)$ is the fourth-order damage stiffness tensor. $\mathbb{C}(\omega)$ can be further expressed as $(1 - \omega)\mathbb{C}_o$ by taking the isotropic damage assumption.

Note that it is critical to obtain the form of macroscopic stress and its relationship with local mechanical responses. According to the principle of virtual power (the total strain energy equates to the sum of the volume averages of strain energies inside and outside the band), more restrictive boundary equilibrium conditions are derived as in Eq. (4) due to satisfying with any arbitrary admissible $d\varepsilon_o$, $d\varepsilon_i^d$, and $[\mathbf{du}]$.

$$\boldsymbol{\Sigma} = \xi \boldsymbol{\sigma}_i + (1 - \xi) \boldsymbol{\sigma}_o \tag{4a}$$

$$\boldsymbol{\Sigma} = \boldsymbol{\sigma}_i \tag{4b}$$

$$\boldsymbol{\Sigma} \bullet \mathbf{n} - \boldsymbol{\sigma}_i \bullet \mathbf{n} = 0 \tag{4c}$$

3 Constitutive model for quasi-brittle rocks

As described in the previous section, the damage and plastic deformation in rocks transfers from diffused/homogeneous to localized/inhomogeneous under loading condition. For the homogeneous state (before localization), it is reasonable to assume volume fraction of the band $\xi = 1$, and the whole rock material can be considered in the band. While after the onset of localization, ξ should be decreased with the increasing of localized damage [15]. Therefore, in this section, for establishing the constitutive model of quasi-brittle rocks, we first propose specific criteria to describe the evolution of the plastic deformation and damage in the localization band, and then the onset of localization condition and the variation of ξ are considered.

3.1 Plastic and damage criteria in localization band

The yield criterion is the constraint condition of global strength relation of local responses. It is noted that the current linear strength criteria (such as Mohr–Coulomb criterion and Drucker-Prager criterion) are not generally enough to be suitable for a wide range of stress condition, especially for the unilateral effect of rocks. For quasi-brittle rocks, the Hoek–Brown strength criterion is more adaptable [38]. According to Eq. (4), we can see that there is no stress jump across the discontinued band. Therefore, it is reasonable to propose a modified Hoek–Brown (MHB) strength-based yield criterion to describe the plastic behavior inside the localization band.

$$f_p(\sigma_i, \omega) = \sigma_{i,1} - \sigma_{i,3} - \eta \frac{\alpha(\omega)}{\alpha_{max}(\omega)} \left(\frac{\sigma_{i,3} + C_o}{p_0} \right)^m \tag{5}$$

where $\sigma_{i,1}$ and $\sigma_{i,3}$ are, respectively, the maximum and minimum principal stress inside the localization band. η , C_o , and m are strength parameters. To ensure the dimensional uniformity, the unit of parameter η is MPa and p_0 equals to 1.0 MPa. $\alpha(\omega)$ is a damage-related function, $\alpha_{max}(\omega)$ is the maximum value of $\alpha(\omega)$. In order to reflect the pre-peak strain hardening and post-peak strain softening behaviors of rocks, the function $\alpha(\omega)$ should satisfy two conditions: (1) should at least C1 continuously differentiable, and (2) should increase first and then decreases with the accumulation of damage. To this end, the following damage hardening/softening function $\alpha(\omega)$ is introduced

$$\alpha(\omega) = 1 - \omega + \frac{2\omega/\omega_c}{1 + (\omega/\omega_c)^2} \tag{6}$$

where ω_c is a damage parameter, which controls the rate of strain hardening and softening behaviors. One can see from Fig. 3 that there is only one peak point of these curves within the range of damage [0, 1]. The hardening or softening rate increases with decreasing of the parameter ω_c while ductile behavior is more obvious with increasing of the parameter ω_c .

From the viewpoint of localization, the homogeneity of the continuum is lost when the localization condition is satisfied. The constitutive behaviors outside and inside the localization band obey independently the generalized Hooke’s law and elastoplastic damage theory. It is noted that the associated plastic flow may overestimate the volumetric dilatancy of quasi-brittle rocks in classical macroscopic plastic models. As one highlights in this study, the plastic evolution in this model can be determined with the associated plastic flow ($G = f_p$) by considering the localization effect. The need for the construction of plastic potential function is bypassed.

$$d\epsilon_i^p = \lambda_p \frac{\partial f_p}{\partial \sigma_i} \tag{7}$$

where λ_p is the non-negative plastic multiplier.

For the sake of simplicity, the isotropic damage assumption is adopted in this study. Inspired by previous studies [31, 33], an exponential damage criterion in Eq. (8) is applied to describe the damage evolution.

$$f_d(Y_d, \omega) = \omega_{\max} \{1.0 - \exp[-\langle Y_d - Y_o \rangle]\} - \omega \tag{8}$$

where ω_{\max} is the maximum damage value and controls the rate of damage evolution. $\langle \cdot \rangle$ is the Macauley bracket, i.e., $\langle x \rangle = (x + |x|)/2$. Damage-driven force Y_d is composed of

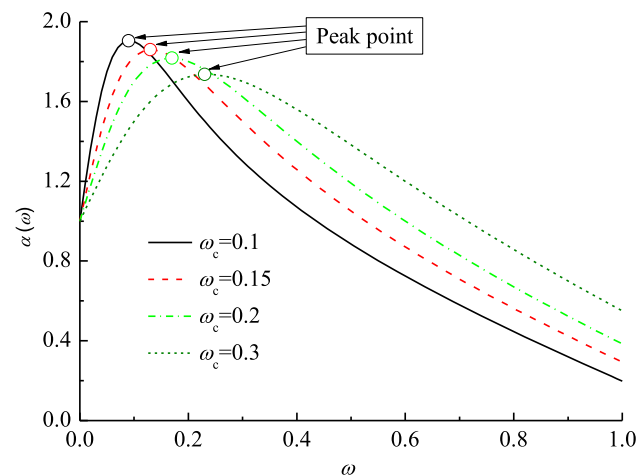


Fig. 3 The relationship of plastic strain hardening/softening function versus the parameter ω_c

the elastic part Y_d^e and plastic part $Y_d^p = \beta\gamma_i^p$, similar to the literature [1]. The competing regimes of plasticity and damage, which one is the inducer, remain an open issue. The threshold Y_o is assumed to equate Y_d^e in order to ensure that the plasticity and damage occur simultaneity in this study.

Similar to the plastic theory, the damage variable increment is defined by

$$d\omega = \lambda_d \frac{\partial f_d}{\partial Y_d} \tag{9}$$

where λ_d is the non-negative plastic multiplier.

3.2 The onset of localization condition

The occurrence and evolution of localized damage are the key factors leading to rock fracture failure. We consider that the onset of localization is a consequence of accumulation of damage. As shown in Eq. (5), when damage reaches a critical value ω_{cr} , the damage hardening/softening function $\alpha(\omega)$ reaches its maximum value $\alpha_{\max}(\omega)$ leading to a material softening. In this case, the corresponding critical damage value can be determined by the condition of $\frac{\partial \alpha(\omega)}{\partial \omega} \Big|_{\omega=\omega_{cr}} = 0$.

$$\omega = \omega_{cr} = \sqrt{\omega_c \left[-(1 + \omega_c) + \sqrt{1 + 4\omega_c} \right]} \tag{10}$$

Accordingly, Eq. (10) seems physically sound to be regarded as the onset of localization condition (similar to our previous work [43]). After the onset of localization, the evolution of the localization zone is governed by the microstructures of materials. Nguyen [15] revealed that localization band is in a contraction process with the increasing of localized damage. To this end, the following condensed relation is empirically introduced to describe the evolution of localization band during the whole loading.

$$\xi = \exp[-\zeta \langle \omega - \omega_{cr} \rangle] \tag{11}$$

where ζ is a model parameter controlling the rate of contraction of the localization band. The Macauley brackets $\langle \cdot \rangle$ are used to control the transition from the plastic/damage homogenization to localization. The sensitivity analysis of parameter ζ is presented in Fig. 4. The results indicate that the rate of contraction of bandwidth increases with the increasing of ζ .

3.3 Incremental constitutive relationship

The incremental form of constitutive model needs to be derived in order to describe and analyze the nonlinear deformation behavior of quasi-brittle rocks. The constitutive relation can be described by the generalized Hooke’s

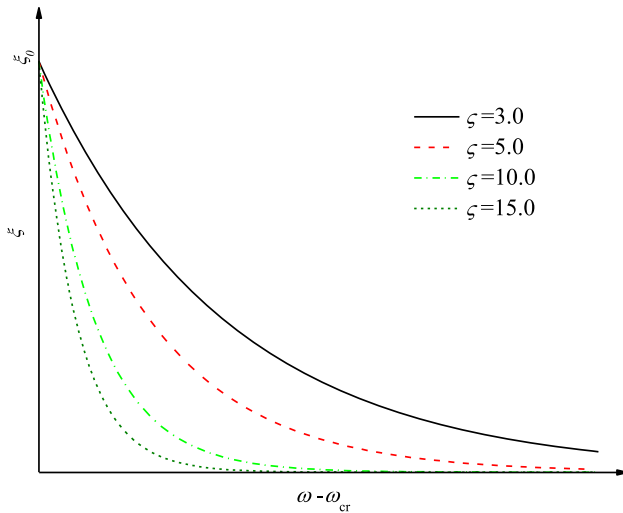


Fig. 4 The localization bandwidth variation law of exponential function

law when the stress state is at elastic stage ($f_p(\sigma_i, \omega) < 0$). The macroscopic stress–strain increment needs to be further derived when the stress state lies on or outside the yield surface. Since the macroscopic strain is applied, the macroscopic incremental stress–strain relationship is inspired by the method in our previous studies [33] and considers the local size effect on the tangent stiffness tensor.

According to the continuous stress across the localization band (in Eq. (4)), the macroscopic stress increment can be expressed as follows

$$d\Sigma = d\sigma_i = d\sigma_o = \mathbb{C}_o : d\varepsilon_o \tag{12}$$

Combining with the condition $\mathbb{C}_o : d\varepsilon_o = \mathbb{C}(\omega) : d\varepsilon_i^{cd}$, the local damage strain ε_i^d in the band can further be derived as expression as follows:

$$d\varepsilon_i^d = \frac{\omega}{1 - \omega} d\varepsilon_o \tag{13}$$

Besides, the elastic strain tensor can be further written by substituting Eqs. (3) and (4) into Eq. (2).

$$d\varepsilon_o = H_\omega (d\mathbf{E} - \zeta d\varepsilon_i^p) \tag{14}$$

where H_ω represents the relationship between the elastic strain outside band and macroscopic and local plastic strain, given by $H_\omega = \frac{1-\omega}{1-\omega+\zeta\omega}$. Therefore, the macroscopic stress increment can be further expressed as

$$d\Sigma = d\sigma_i = H_\omega \mathbb{C}_o : (d\mathbf{E}\mathbf{g}; - \zeta d\varepsilon_i^p) \tag{15}$$

When the yield condition is satisfied, the differential formulas of plastic consistency condition are written as

$$f_p = \frac{\partial f_p}{\partial \sigma_i} d\sigma_i + \frac{\partial f_p}{\partial \gamma_i^p} d\gamma_i^p = 0 \tag{16a}$$

$$f_p = H_\omega \frac{\partial f_p}{\partial \sigma_i} : \mathbb{C}_o : (d\mathbf{E} - \zeta d\varepsilon_i^p) + \frac{\partial f_p}{\partial \omega} \frac{\partial \omega}{\partial \gamma_i^p} d\gamma_i^p = 0 \tag{16b}$$

To simplify the derivation of the formula, $H_{\sigma\varepsilon}$ and H_γ are, respectively, defined as $H_{\sigma\varepsilon} = \frac{\partial f_p}{\partial \sigma_i} : \mathbb{C}_o : \frac{\partial f_p}{\partial \sigma_i}$ and

$$H_\gamma = \frac{\partial f_p}{\partial \omega} \frac{\partial \omega}{\partial \gamma_i^p} \sqrt{\frac{2}{3} \text{dev} \left(\frac{\partial f_p}{\partial \sigma_i} \right) : \text{dev} \left(\frac{\partial f_p}{\partial \sigma_i} \right)}$$

. Then the plastic multiplier is derived by solving Eq. (16).

$$d\lambda_p = \frac{H_\omega \frac{\partial f_p}{\partial \sigma_i} : \mathbb{C}_o : d\mathbf{E}}{\zeta H_\omega H_{\sigma\varepsilon} - H_\gamma} \tag{17}$$

Therefore, the macroscopic stress–strain relationship can be derived as

$$d\Sigma = d\sigma_i = \mathbb{C}_{ep} : d\mathbf{E} \tag{18}$$

with the tangent stiffness tensor \mathbb{C}_{ep}

$$\mathbb{C}_{ep} = \begin{cases} \mathbb{C}_o & , \text{if } f_p(\Sigma, \omega) < 0 \\ H_\omega \left[\mathbb{C}_o - \frac{\zeta H_\omega \mathbb{C}_o : \left(\frac{\partial f_p}{\partial \sigma_i} \otimes \frac{\partial f_p}{\partial \sigma_i} \right) : \mathbb{C}_o}{\zeta H_\omega H_{\sigma\varepsilon} - H_\gamma} \right] & , \text{if } f_p(\Sigma, \omega) \geq 0 \end{cases} \tag{19}$$

It is noted that the localization effect is inherently considered in the constitutive model by introducing the parameter ζ into \mathbb{C}_{ep} . The local plastic and damage variables still need to be solved iteratively to update the mechanical variables in Sect. 4.

4 Computational procedures

In the numerical implementation process, the constitutive model needs to be further expressed in incremental formulation and implemented in computer code based on the Sect. 3. And we also need to calculate the intermediate variables (such as plasticity and damage multipliers) in the updating process of the mechanical variables. In order to simulate the complete mechanical responses (especially in the post-peak regime), the displacement-driven is adopted by analogy to the laboratory test. In order to facilitate the numerical implementation in the finite element method (FEM), the plasticity and damage multipliers are given during numerical updating in this section.

Return rapping algorithm proposed by Simo and Hughes [25], has been widely applied to solve the problem of

nonlinear numerical iteration solution. The stress updating algorithm contains two parts: elastic prediction and nonlinear corrections (including plasticity and damage). The key idea of this method is to return the stress state back the yield plane by obtaining the real strain tensor through iteration correction when stress is beyond the yield surface. Therefore, the trial stress tensor σ_i^{trial} is calculated by applying a trial strain increment $d\mathbf{E}$ at first and then check whether the stress state exceeds the yield surface. The generalized Hooke’s law is used to calculate the elastic constitutive relation when the condition $f_p(\sigma_i, \omega) < 0$ is satisfied. While nonlinear correction is adopted to make the stress state regress to the yield and damage surfaces when the plastic condition $f_p(\sigma_i, \omega) \geq 0$ and damage condition $f_d(Y_d, \omega) \geq 0$ are satisfied. Internal variables, yield and damage functions are also updated in each iteration step. Note that the damage condition is automatically satisfied when the plasticity condition is satisfied since damage and plasticity occur simultaneously in this model in Sect. 3. Therefore, it is only necessary to judge whether yield condition is satisfied at the point of Gauss integration by the yield function in Eq. (5).

4.1 Elastic prediction

The stress and strain tensors inside band are equal the corresponding trial mechanical variables when the trial stress is below the yield surface ($f_p(\sigma_i, \omega) < 0$). The macroscopic mechanical variables are equivalent to the local mechanical responses due to $\xi = 1.0$ at the $(k + 1)$ th step, updated as follows:

$$\Sigma^{k+1} = \sigma_i^{k+1} = \sigma_i^{trial} = \sigma_i^k + d\sigma_i^{k+1} \tag{20a}$$

$$\mathbf{E}^{k+1} = \varepsilon_i^{k+1} = \varepsilon_i^{trial} = \varepsilon_i^k + d\mathbf{E}^{k+1} \tag{20b}$$

And the macroscopic stress increment can be calculated according to the generalized Hooke’s law.

$$d\sigma_i^{k+1} = \mathbb{C}_o : d\mathbf{E} \tag{21}$$

4.2 Nonlinear corrections

The plastic and damage corrections can be, respectively, obtained by making use of the first-order Taylor expansion of plastic and damage consistency conditions when $f_p(\sigma_i, \omega) \geq 0$, as follows

$$f_{p,j+1}^{k+1} = f_{p,j}^{k+1} + \frac{\partial f_{p,j}^{k+1}}{\partial \sigma_{i,j+1}^{k+1}} \delta \sigma_{i,j+1}^{k+1} + \frac{\partial f_{p,j}^{k+1}}{\partial \omega_j^{k+1}} \frac{\partial \omega_j^{k+1}}{\partial \gamma_{i,j}^{p,k+1}} \delta \gamma_{i,j}^{p,k+1} \approx 0 \tag{22a}$$

$$f_{d,j+1}^{k+1} = f_{d,j}^{k+1} + \frac{\partial f_{d,j}^{k+1}}{\partial \omega_j^{k+1}} \delta \omega_j^{k+1} \approx 0 \tag{22b}$$

where

$$\delta \sigma_{i,j+1}^{k+1} = -\xi H_{\omega_j}^{k+1} \mathbb{C}_o : \delta \varepsilon_{i,j}^{p,k+1} \tag{23a}$$

$$\delta \varepsilon_{i,j}^{p,k+1} = \delta \lambda_p \frac{\partial f_{p,j}^{k+1}}{\partial \sigma_{i,j}^{k+1}} \tag{23b}$$

$$\delta \gamma_{i,j}^{p,k+1} = \delta \lambda_d \sqrt{\frac{2}{3} \text{dev} \left(\frac{\partial f_{p,j}^{k+1}}{\partial \sigma_{i,j}^{k+1}} \right) : \text{dev} \left(\frac{\partial f_{p,j}^{k+1}}{\partial \sigma_{i,j}^{k+1}} \right)} \tag{23c}$$

$$\delta \omega_j^{k+1} = \delta \lambda_d \frac{\partial f_{d,j}^{k+1}}{\partial Y_{d,j}^{k+1}} \tag{23d}$$

where $\delta \lambda_p$ and $\delta \lambda_d$ are, respectively, plastic multiplier and damage multiplier. j is number of internal iteration and “ δ ” represents the tiny increment between iteration steps.

$$\delta \lambda_p = \frac{f_{p,j}^{k+1}}{\xi H_{\omega_j}^{k+1} H_{\sigma_{\varepsilon,j}}^{k+1} - H_{\gamma_j}^{k+1}} \tag{24a}$$

$$\delta \lambda_d = \frac{f_{d,j}^{k+1}}{\omega_c \exp \left[-\left\langle Y_{d,j}^{k+1} - Y_o \right\rangle \right]} \tag{24b}$$

Finally, the mechanical variables (such as stress and strain) are updated as the following formulas:

$$\Sigma^{k+1} = \sigma_i^{k+1} = \sigma_i^{trial} + \sum_{j=1}^{j=iter} \delta \sigma_{i,j+1}^{k+1} \tag{25a}$$

$$\varepsilon_i^{k+1} = \varepsilon_i^{trial} + \sum_{j=1}^{j=iter} \delta \varepsilon_{i,j}^{p,k+1} \tag{25b}$$

where $iter$ represents the inner maximum iteration number satisfying the external iteration convergence.

The macroscopic strain is further updated by the following form.

$$\mathbf{E}^{k+1} = \xi \varepsilon_i^{k+1} + (1 - \xi) \varepsilon_o^{k+1} \tag{26}$$

In order to intuitively illustrate the updating of mechanical variables and the numerical iteration process, the flowchart of numerical implementation is shown in Fig. 5. Note that all mechanical variables are known at the end of k step and strain-controlled procedure is adopted with a constant strain increment $d\mathbf{E}$ in this study.

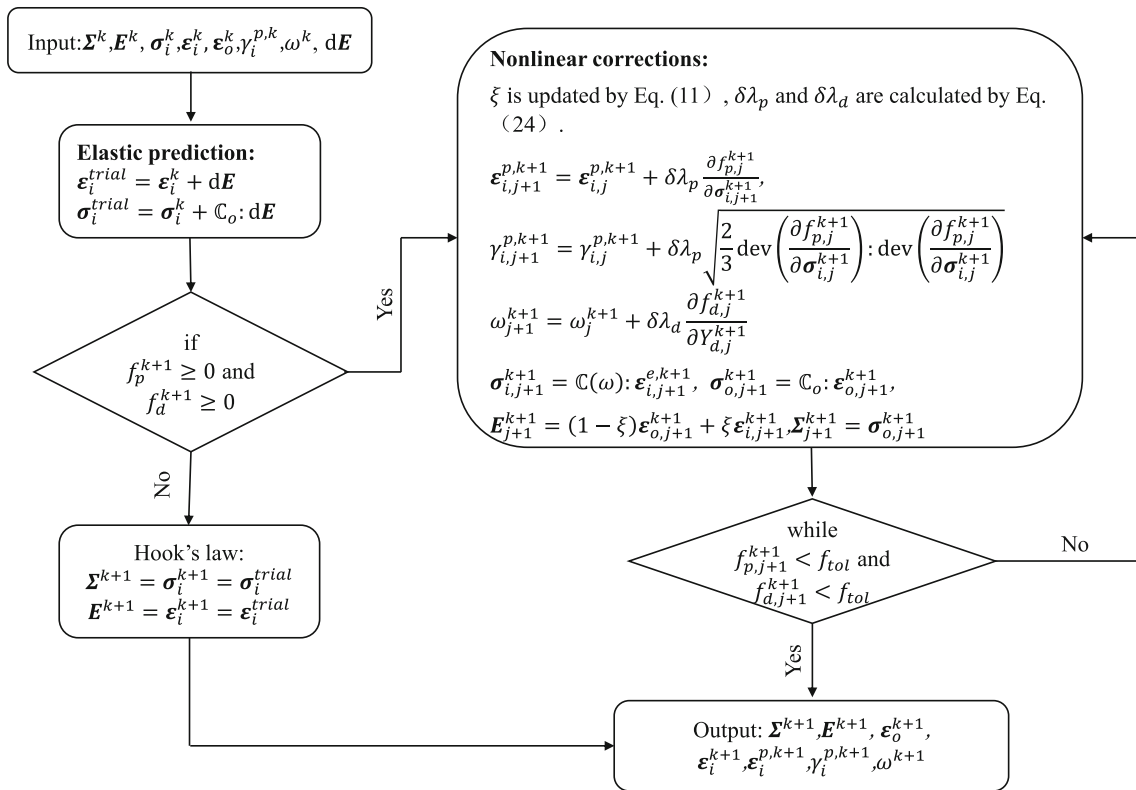


Fig. 5 Schematic chart of the iteration algorithms in numerical implementation (f_{tol} is allowable error of convergence ($f_{tol} = 10^{-3}$))

5 Parameters identification and model verification

5.1 Model parameters identification method

There are nine model parameters of the proposed model. All of them can be calibrated directly or indirectly according to the triaxial test data. Elastic parameters: elastic modulus E and Poisson’s ratio ν are the physical properties, which can be directly obtained by the slope of linear stage of stress–strain curves. Plastic parameters η and m can be directly obtained by fitting the peak strength with the MHB criterion due to the associated plastic flow adopted in this study. Damage parameters ω_c and β are obtained by indirect inverse calibration, which correspond to the values when the optimal fitting results with test data by the repeated numerical simulations. The damage parameter ω_{max} can be determined based on the triaxial cyclic loading test data analysis. Due to localization band evolving with the confining pressure, ω_{max} is further calibrated by fitting with test data when the corresponding test results are lacked. The localization parameter ς is determined with the help of the advanced technology, such as acoustic emission (AE) and digital image correlation (DIC). The aim is to obtain the spatial and temporal distribution information of localization band. Unfortunately,

most of the existing test results focus on qualitative description and lack of quantitative analysis. Parameters β and ς mainly affect the nonlinear mechanical behaviors of the model and are not readily available. Therefore, the sensitivity of the two model parameters should be carried out in order to understand their mechanical influences on the model. The related study is carried out in the following section with red sandstone. Then the two model parameters can be determined by repeated trail calculation and comparing with the simulation results and test data.

5.2 Red sandstone

Sandstone (widely distributed in the earth’s crust) is a typical sedimentary rock material. In order to simulate the deep rock mechanical behaviors, a series of triaxial compression tests of red sandstone were conducted under the various confining pressure of 5, 20, 35, 50, and 65 MPa by Yang [38]. All of samples are characterized by the brittle failure, even at high confining pressure of 50 and 60 MPa. The strength envelope of the rock is shown in Fig. 6. The results indicate that the MHB criterion can accurately capture the peak strength under the entire stress condition. Because the elastic parameters of red sandstone changes with the confining pressure, the two parameters are considered the confining pressure effect and given as the same

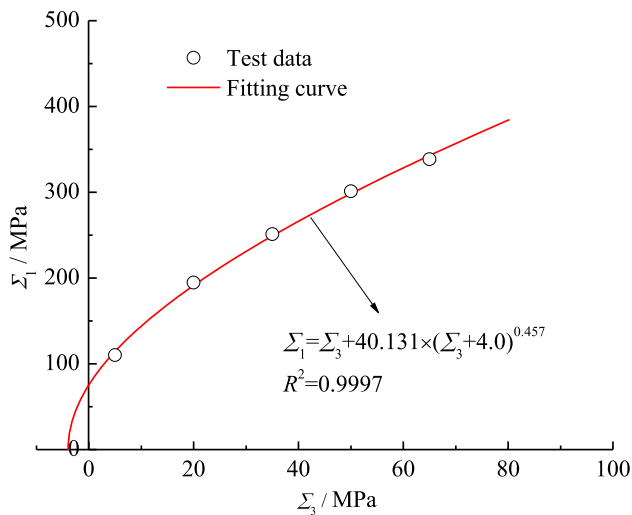


Fig. 6 Strength envelope of red sandstone fitted based on test peak strength (R^2 is correlation coefficient)

Table 1 The model parameters for red sandstone

Confining pressure Σ_3 /MPa	Plastic parameters			Damage parameters		
	η /MPa	m	C_o	ω_c	β	ω_{max}
5	40.131	0.457	4.0	0.2	75.0	0.65
20						0.60
35						0.55
50						0.50
65						0.45

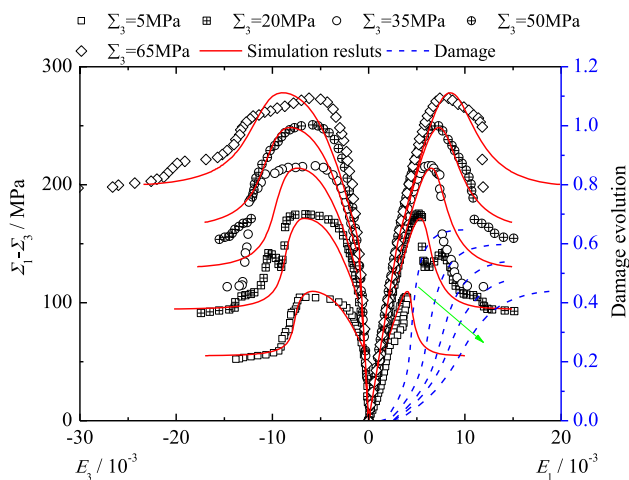


Fig. 7 The comparison between numerical simulation results and the test data of red sandstone

in the published literature. The plastic and damage parameters are presented in Table 1. Besides, $\zeta = 3.0$ is

adopted to control the decreasing of localization band according to the repeated numerical trial.

Figure 7 presents the comparison results between simulation results and test data. The cracks propagation inhibited with increasing of confining pressure can be reflected through damage evolution. The green arrows in Fig. 7 indicate that damage evolution changes with the increasing of confining pressure. That is, the degree and evolution rate of damage decrease with increasing of confining pressure. Moreover, we can see that the law of damage evolution is similar to the trend of AE counts accumulation in the published literature. The simulation results are in good agreement with test data, which indicate that the proposed model can capture the mainly nonlinear mechanical behaviors, not only the pre-peak strain hardening behavior but also the strain softening behavior once the stress exceeds the peak stress. Moreover, the strain softening phenomenon is the result of the accelerated accumulation of damage evolution.

The effect of parameter ω_c is introduced in Sect. 3. In order to obtain the effect of parameter β on the responses of the proposed model, the sensitivity analysis is conducted in Fig. 8. The arrow in the figure indicates the parameter increases. The results indicate that the parameter β influences the strain hardening/softening rate, which increases with increasing of β . Figure 9 presents the sensitivity analysis of the parameter ζ . The results indicate that the parameter ζ only influences the post-peak strain softening rate, which increases with increasing of ζ . Note that the parameters β and ζ do not affect the peak strength during numerical simulation, but only affect the nonlinear deformation behavior. This is also a feature of the proposed model.

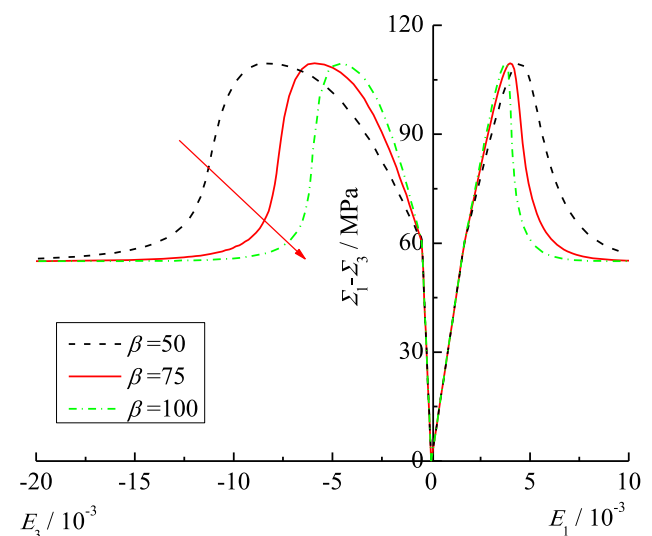


Fig. 8 The parameter sensitivity analysis of β ($\Sigma_3 = 5$ MPa)

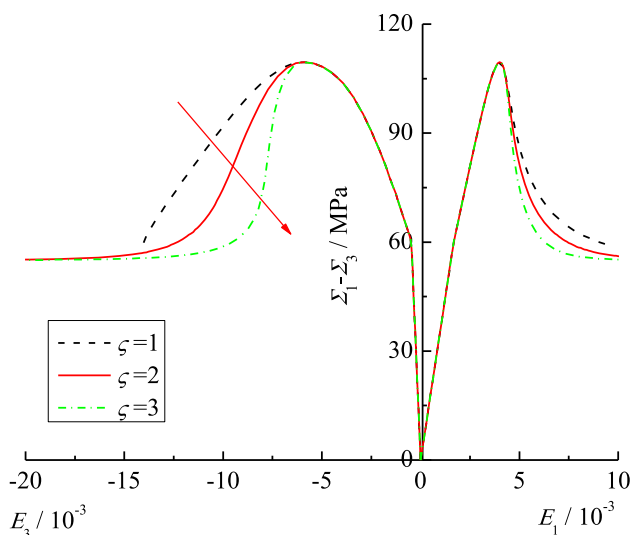


Fig. 9 The parameter sensitivity analysis of ζ ($\Sigma_3 = 5\text{MPa}$)

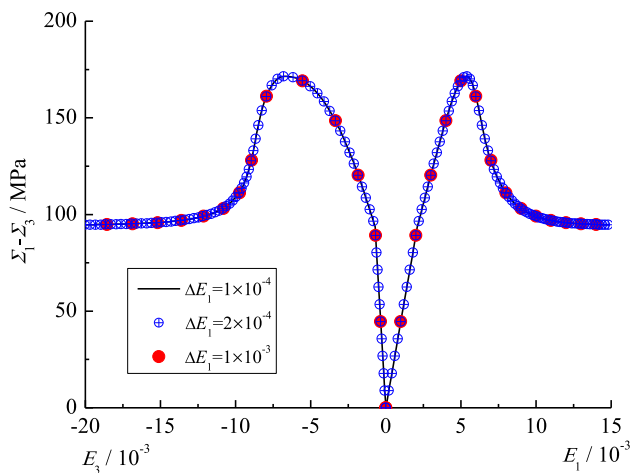


Fig. 10 The effect of loading step on the numerical results

In order to illustrate the robustness of numerical algorithms, the influence of loading step on the simulation results is plotted under various loading rates in Fig. 10. The confining pressure is set as 20 MPa and the other model parameters are chosen the same values from Table 1, expect for the loading step changes. The results indicate that all the numerical simulation points are basically on the same outline. That is to say, the numerical results are independent of the size of loading step, which directly validate the robustness of the algorithm.

5.3 Kuru granite

A series of triaxial compression tests of Kuru granite were conducted under confining pressure changing from 0 to 75 MPa [28]. And the average tensile strength of the rock is 11.4 ± 2 MPa estimated by 14 samples with the

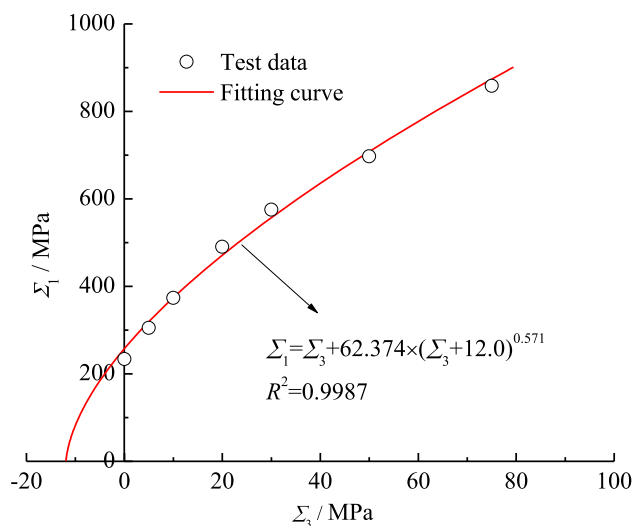


Fig. 11 Strength envelope fitting based on test peak strength of Kuru granite

Table 2 The model parameters for Kuru granite

Confining pressure Σ_3/MPa	Plastic parameters			Damage parameters		
	η/MPa	m	C_o	ω_c	β	ω_{\max}
0	62.374	0.571	12.0	0.1	120	0.5
5					50	
10						
20						
30						
50						
75						

Brazilian test. The experimental curves can be seen that at Class II failure is founded for the brittle rock with an obvious snapback behavior at the post-peak stage. Based on the peak strength of the rock, the strength envelope of MHB criterion is drawn in Fig. 11. The results indicate the criterion can be better describe the relationship between failure stress and confining pressure. The uniaxial strength of the rock is slightly overestimated by the proposed criterion. The required model parameters are presented in Table 2 as given method in Sect. 5.1. It is worth noting that the spalling failure (the failure plane is along the direction of maximum principal stress) of the rock is in uniaxial compression test. The brittleness and the localized failure degree of rock are higher under uniaxial compression test. Therefore, the damage parameter β is considered independently in the uniaxial compression test. $\zeta = 8.0$ is adopted to control the decreasing of localization band according to the repeated numerical trial.

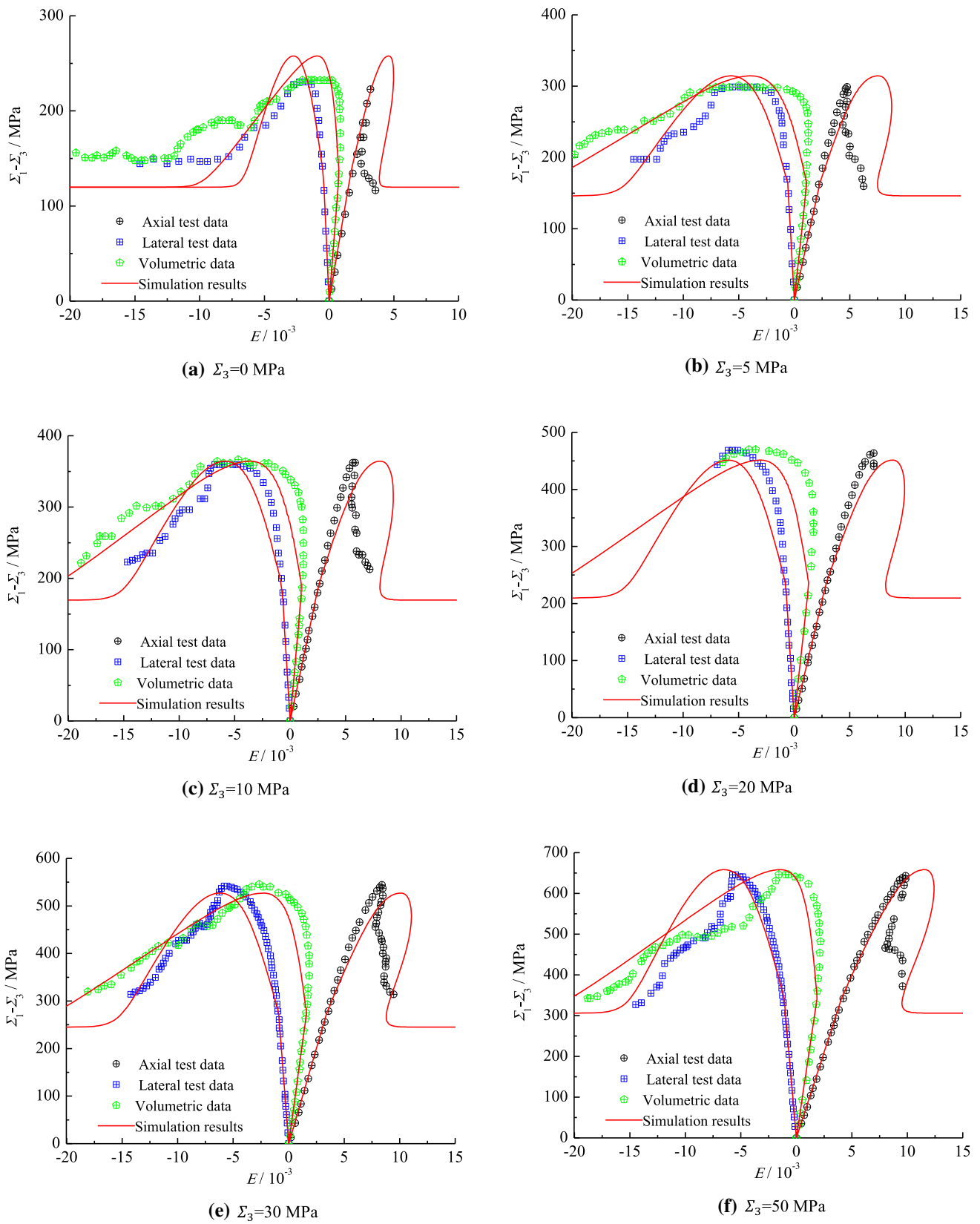


Fig. 12 The comparison between numerical simulation results and the test data of Kuru granite

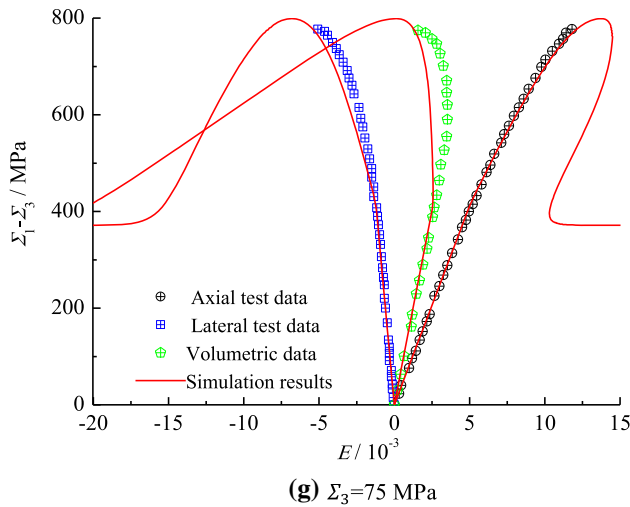


Fig. 12 continued

In order to obtain the complete test curves at the post-peak stage, the circumferential strain-controlled mode is applied in the numerical simulation. The comparison results between simulation results and uniaxial and triaxial compression test of the rock are presented in Fig. 12. Although there are some errors in numerical simulations, the main mechanical responses of Kuru granite can be reflected by the proposed model on the whole. The discrepancy of the deviatoric stress versus axial strain curve is somewhat overvalued since the isotropic damage assumption is adopted. In fact, cracks evolution influenced by the unequal stress condition will propagate along a dominant direction. As a result, the axial damage evolution is overestimated to some extent in numerical simulation results. Therefore, a refined model will be further considered stress-induced anisotropic damage in future.

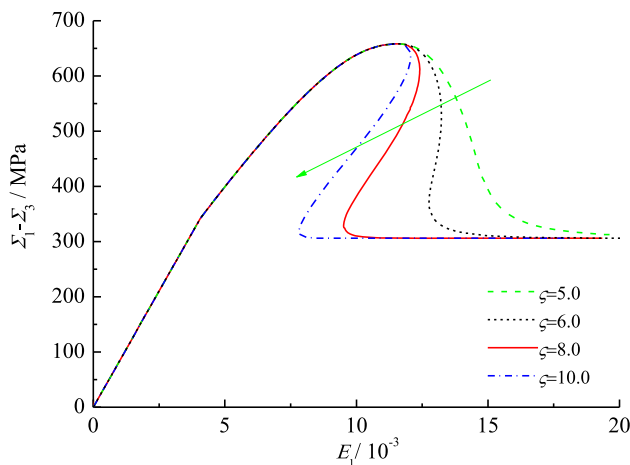


Fig. 13 The sensitivity analysis of post-peak responses of Kuru granite under confining pressure of 50 MPa in the numerical simulation (the direction of the arrow means the increase of ζ)

The post-localization responses are simulated through changing with the parameter ζ in Fig. 13. An interesting phenomenon can be seen that the post-peak is sensitive with respect to ζ . As discussed in Sect. 3, the increasing of the parameter ζ means that the localized failure degree is accelerated. Therefore, the localization effect plays an important role in the post-peak snapback behavior. The magnitude of stress drop increases with increasing of ζ , and the post-peak snapback phenomenon is more obvious. While the phenomenon may not occur when localization effects are ignored or the decreasing of localization bandwidth is at a low rate. In other words, compared with the conventional constitutive model, the proposed model is more reasonable to capture the mechanical behaviors of heterogeneous rocks. Therefore, we can see that the Class II failure of brittle rocks is the result of the localization in the post-peak regime and the traditional constitutive model ignoring the local effect (ξ keeps constant) cannot capture the underlying physical mechanism of snapback characteristics.

5.4 Low-porosity sandstone

The comparison between numerical simulation and the test data of low-porosity sandstone is performed in this section to validate the capability of the proposed constitutive model. A series of triaxial compression tests of sandstone were conducted under various of confining pressures ranging from 0 to 120 MPa [10]. The test results indicate that the transition from brittle failure to cataclastic flow regime in the rock is founded with increasing of confining pressure. The failure faulting is observed when the confining pressure changes from 0 to 50 MPa, while ductile deformation is shown when the confining pressure changes

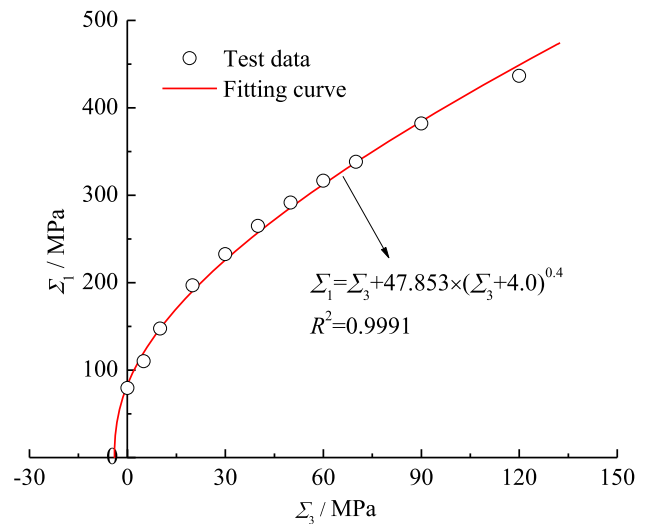


Fig. 14 Strength envelope fitting based on test peak strength

Table 3 The model parameters for sandstone

Confining pressure Σ_3 /MPa	Plastic parameters			Damage parameters		
	η /MPa	m	C_o	ω_c	β	ω_{max}
0	47.853	0.4	4.0	0.2	100.0	0.60
5						0.50
10						0.40
20						0.35
30						0.32
50						0.26
60						0.25
90						0.22
120						0.20

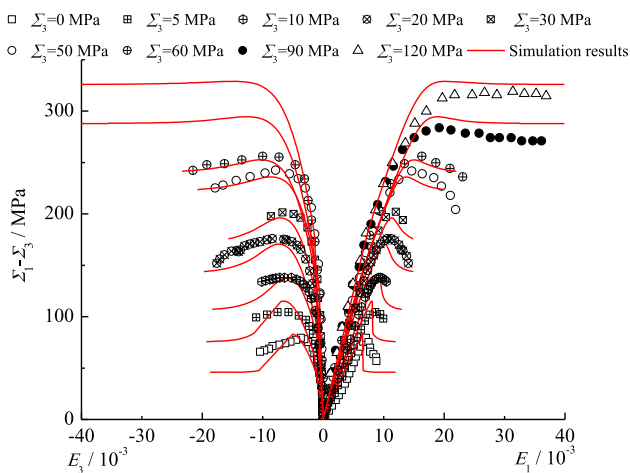


Fig. 15 The comparison between numerical simulation results and the test data

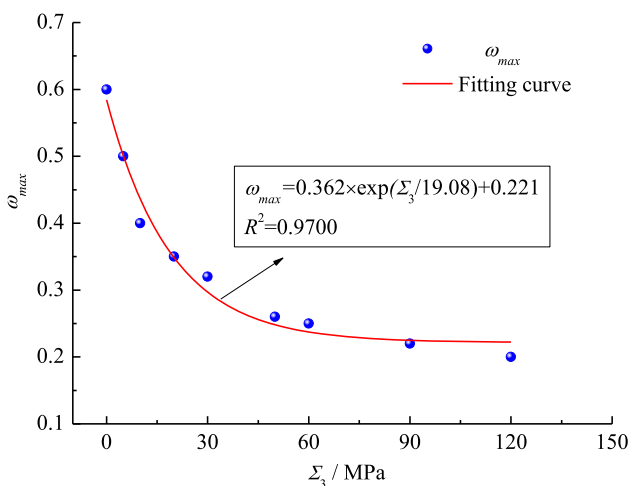


Fig. 16 The variation of parameter ω_{max} with increasing confining pressure

from 60 to 120 MPa. The strength envelope of the sandstone is fitted by the MHB criterion in Fig. 14. A good consistency between fitting results and peak strength validate that the proposed criterion can describe the strength relations during a wide range of compression stress conditions.

Based on the test data of sandstone, the required model parameters are presented in Table 3. $\zeta = 1.5$ is adopted to control the decreasing of localization band according to the repeated numerical trial. Note that the snapback may be induced when the ζ_0 is smaller or the reduction rate of the localization band is too fast.

The numerical verification by comparing with typical test data ($\Sigma_3 = 0, 5, 10, 20, 30, 50, 60, 90,$ and 120 MPa) is plotted in Fig. 15. The results indicate the simulation results match well with the experimental characteristics of the sandstone under compression condition. The overall mechanical responses can be reproduced by the proposed model. Especially, the localization brittle failure under low confining and ductile deformation can also be captured by giving a suitable damage parameter ω_{max} . The relationship between ω_{max} and σ_3 can be fitted by an expansional function (in Fig. 16). The aim is to reflect ductile deformation and cataclastic flow under high confining pressure by reducing the rate damage evolution, which is validated by our previous studies [31]. Moreover, the plastic deformation of sandstone can be well corrected by considering the localization effect in the plastic potential.

Note that pore collapse and grain crushing may become the dominant failure mechanisms under the higher confining pressure, which can be captured by considering the evolving of porosity in yield criterion [24] or introducing a new yield function [35]. The corresponding studies have not been involved this work. In order to match the simulation results with the experimental data, the damage

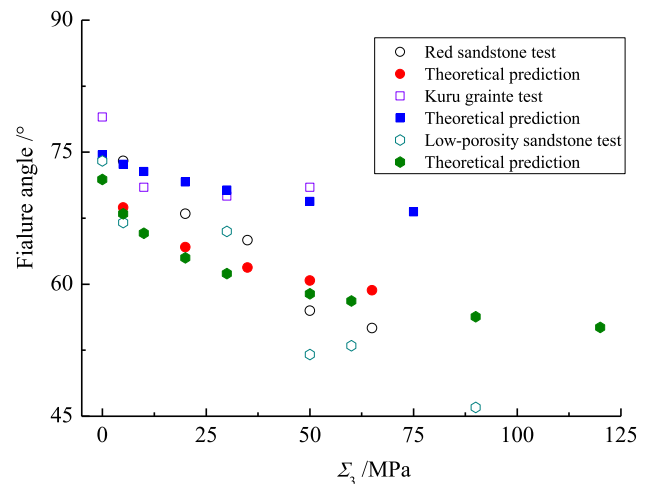


Fig. 17 The comparison of failure angles between theoretical prediction and experimental observation

parameter ω_{\max} is taken different under various confining pressure for sandstone. As for hard rocks (such as granite), the pore collapse and grain crushing mechanisms can be ignored. Therefore, a constant ω_{\max} is chosen for the granite. Moreover, the propagation law of the localization band is empirically given with the function of damage. This process is also affected by the stress condition. The more precise formulation needs to be modified in combination with further test results.

Besides, the prediction of the orientation of failure plane angle is also an important basis for checking the effectiveness of localized damage model. The determination method of failure angle θ_c at peak point can refer to “Appendix A.” The comparison results between theoretical predictions and experimental observation of red sandstone, Kure granite, and low-porosity sandstone are presented in Fig. 17. The results indicate that the prediction ability of the model is fully demonstrated in the case of shear failure, while the failure angle is underestimated under the uniaxial compression condition and is overestimated under the high confining pressure. The reason is that the uniaxial tensile fracture mechanism and the pore collapse mechanism under high confining pressure of rock are neglected in the proposed model.

6 Conclusions

This work introduces the description approach of localization regime of quasi-brittle rocks at the constitutive model level. Specific criteria are proposed to describe the evolution of the plastic and damage in the localization band. The onset of localization condition is also derived. The plastic and damage behaviors are assumed inside the localization zone and elastic deformation is considered outside the zone. Consequently, the macroscopic responses are obtained by using a volume average procedure incorporating the evolution of the volume fraction of the localization zone.

The transition from diffused deformation to localized failure is reflected by considering the embedded localization effects in the associated plastic potential. The post-peak snapback and brittle-ductile transition behaviors of rock are characterized through the variation of localization size parameter with confining pressure. Damage variable is used to control the contraction and expansion of the yield surface in order to capture the pre-peak strain hardening and post-peak strain softening behaviors. The main model parameters with clear physical meaning can be identified directly or indirectly according to triaxial test data. The capability of the proposed model in predicting mechanical responses of quasi-brittle rocks are proven by a good agreement between simulation results and the triaxial

compression test data of red sandstone, Kuru granite, and low-porosity sandstone. The robustness of the numerical algorithm is also validated by comparing the simulation results under various loading steps. Moreover, the drawback of overestimating the plastic deformation of geomaterials in the classical plasticity is also overcome.

Due to limitations of local stress field monitoring in laboratory test, the validity of the proposed model still needs to be further checked with other test results of quasi-brittle rocks by the advanced scientific and technology. Moreover, it is difficult to reflect the complex fracture forms of quasi-brittle rocks due to only one localization band was assumed in this work. Further studies will focus on extending the localized model considering the anisotropic damage evolution, which is used to describe the orientation of cracks propagation depending on the stress condition.

Appendix

Derivation of failure angle

Combining with Eqs. (4) and (5), one can derive the following HMB macroscopic strength criterion

$$F(\Sigma) = \Sigma_1 - \Sigma_3 - \eta \left(\frac{\Sigma_3 + C_o}{p_o} \right)^m \quad (27)$$

The slope K of the tangent line of the strength envelope can be derived as

$$K = \frac{\partial \Sigma_1}{\partial \Sigma_3} = 1 + \eta m \left(\frac{\Sigma_3 + C_o}{p_o} \right)^{m-1} \quad (28)$$

The HMB criterion can be understood as the Mohr–Coulomb criterion for the change of the friction angle φ . Therefore, by simple algebraic manipulation, $\tan \varphi$ can be expressed with K , as follows

$$\tan \varphi = \left(\frac{K - 1}{2\sqrt{K}} \right) \quad (29)$$

The friction angle can be further written as

$$\varphi = \arctan \left(\frac{K - 1}{2\sqrt{K}} \right) \quad (30)$$

Finally, the failure angle θ_c can be calculated by

$$\theta_c = \frac{\varphi}{2} + \frac{\pi}{2} \quad (31)$$

Funding This study is financially supported by the National Natural Science Foundation of China (Grant No. 52109143), China Postdoctoral Science Foundation (Grant No. 2022M713376) and the

Fundamental Research Funds for the Central Universities (2021QN1023).

References

- Batiste SN, Alshibli KA, Sture S, Lankton M (2004) Shear band characterization of triaxial sand specimens using computed tomography. *Geotech Test J* 27(6):568–579
- Bruning T, Karakus M, Nguyen GD, Goodchild D (2019) An experimental and theoretical stress-strain-damage correlation procedure for constitutive modelling of granite. *Int J Rock Mech Min Sci* 116:1–12
- Chang J, Li S, Wang W, Niu Q (2021) A study of non-coaxial effects on strain localization via micropolar plasticity model. *Acta Geotechnica* 17:1–19
- Gupta N, Mishra B (2020) Influence of stress-induced microcracks on viscoplastic creep deformation in Marcellus shale. *Acta Geotechnica* 16:1–21
- Haghighat E, Pietruszczak S (2015) On modeling of discrete propagation of localized damage in cohesive-frictional materials. *Int J Numer Anal Meth Geomech* 39(16):1774–1790
- Han B, Xie SY, Shao JF (2016) Experimental investigation on mechanical behavior and permeability evolution of a porous limestone under compression. *Rock Mech Rock Eng* 49(9):3425–3435
- Hu X, Xie N, Zhu Q, Chen L, Li P (2020) Modeling damage evolution in heterogeneous granite using digital image-based grain-based model. *Rock Mech Rock Eng* 53(11):4925–4945
- Jiang Q, Su G, Feng X-T, Chen G, Zhang M-Z, Liu C (2019) Excavation optimization and stability analysis for large underground caverns under high geostress: a case study of the Chinese Laxiwa project. *Rock Mech Rock Eng* 52(3):895–915
- Le LA, Nguyen GD, Bui HH, Sheikh AH, Kotousov A (2018) Localised failure mechanism as the basis for constitutive modelling of geomaterials. *Int J Eng Sci* 133:284–310
- Liu SL, Chen HR, Yuan SS, Zhu QZ (2020) Experimental investigation and micromechanical modeling of the brittle-ductile transition behaviors in low-porosity sandstone. *Int J Mech Sci* 179:105654
- Liu Z, Shao J, Xie S, Conil N, Zha W (2018) Effects of relative humidity and mineral compositions on creep deformation and failure of a claystone under compression. *Int J Rock Mech Min Sci* 103:68–76
- Ma Y, Huang H (2021) Effect of shear bond failure on the strength ratio in DEM modeling of quasi-brittle materials. *Acta Geotechnica* 16(8):2629–2642
- Munoz H, Taheri A (2017) Local damage and progressive localisation in porous sandstone during cyclic loading. *Rock Mech Rock Eng* 50(12):3253–3259
- Munoz H, Taheri A, Chanda EK (2016) Pre-peak and post-peak rock strain characteristics during uniaxial compression by 3D digital image correlation. *Rock Mech Rock Eng* 49(7):2541–2554
- Nguyen GD, Bui HH (2020) A thermodynamics-and mechanism-based framework for constitutive models with evolving thickness of localisation band. *Int J Solids Struct* 187:100–120
- Nguyen NH, Bui HH, Nguyen GD, Kodikara J (2017) A cohesive damage-plasticity model for DEM and its application for numerical investigation of soft rock fracture properties. *Int J Plast* 98:175–196
- Nguyen GD, Einav I, Korsunsky AM (2012) How to connect two scales of behaviour in constitutive modelling of geomaterials. *Géotech Lett* 2(3):129–134
- Nguyen GD, Korsunsky AM, Einav I (2014) A constitutive modelling framework featuring two scales of behaviour: fundamentals and applications to quasi-brittle failure. *Eng Fract Mech* 115:221–240
- Parisio F, Lehmann C, Nagel T (2020) A model of failure and localization of basalt at temperature and pressure conditions spanning the brittle-ductile transition. *J Geophys Res Solid Earth* 125(11):e2020JB050539
- Peng J, Rong G, Yao MD, Wong LNY, Tang ZC (2018) Acoustic emission characteristics of a fine-grained marble with different thermal damages and specimen sizes. *Bull Eng Geol Environ* 78:1–13
- Rabczuk T, Ren H (2017) A peridynamics formulation for quasi-static fracture and contact in rock. *Eng Geol* 225(S1):42–48
- Rudnicki JW, Rice J (1975) Conditions for the localization of deformation in pressure-sensitive dilatant materials. *J Mech Phys Solids* 23(6):371–394
- Shen WQ, Shao JF, Cao YJ, Wang SS, Xu WY (2020) A micromechanics-based enhanced plastic damage model including localization analysis for heterogeneous geomaterials. *Comput Geotech* 122:103512
- Shen W, Shao J-F, Liu Z, Oueslati A, De Saxcé G (2020) Evaluation and improvement of macroscopic yield criteria of porous media having a Drucker-Prager matrix. *Int J Plast* 126:102609
- Simo JC, Hughes TJ (2006) *Computational inelasticity*. Springer, Berlin
- Sirdesai NN, Gupta T, Singh TN, Ranjith PG (2018) Studying the acoustic emission response of an Indian monumental sandstone under varying temperatures and strains. *Constr Build Mater* 168:346–361
- Su Y-C, Sewell T, Chen Z (2021) Comparative investigation of shear-band evolution using discrete and continuum-based particle methods. *Acta Geotechnica* 16(8):2337–2354
- Tkalich D, Fourmeau M, Kane A, Li C, Cailletaud G (2016) Experimental and numerical study of Kuru granite under confined compression and indentation. *Int J Rock Mech Min Sci* 87:55–68
- Walton G, Hedayat A, Kim E, Labrie D (2017) Post-yield strength and dilatancy evolution across the brittle-ductile transition in Indiana limestone. *Rock Mech Rock Eng* 50(4):1–20
- Wang SS, Wang HL, Xu WY, Qian W (2019) Investigation on mechanical behaviour of dacite under loading and unloading conditions. *Géotech Lett* 9(2):130–135
- Wang SS, Xu WY (2020) A coupled elastoplastic anisotropic damage model for rock materials. *Int J Damage Mech* 29(8):1222–1245
- Wang S, Xu W, Jia C, Wang W (2018) Mechanical behavior of fine-grained sandstone in triaxial compression and elastoplastic modeling by return mapping algorithms. *Bull Eng Geol Environ* 77(4):1689–1699
- Wang S, Xu W, Wang W, Jia C (2018) Experimental and numerical investigations on the mechanical behavior of fine-grained sandstone. *Int J Geomech* 18(2):04017150
- Wu J-Y, Cervera M (2015) On the equivalence between traction- and stress-based approaches for the modeling of localized failure in solids. *J Mech Phys Solids* 82:137–163
- Xie S, Shao J (2012) Experimental investigation and poroplastic modelling of saturated porous geomaterials. *Int J Plast* 39:27–45
- Xu Y, Cai M (2017) Influence of loading system stiffness on post-peak stress-strain curve of stable rock failures. *Rock Mech Rock Eng* 50(9):2255–2275
- Yan Z, Wang K, Zang J, Wang C, Liu A (2019) Anisotropic coal permeability and its stress sensitivity. *Int J Min Sci Technol* 29(3):507–511
- Yang S-Q, Jing H-W, Wang S-Y (2012) Experimental investigation on the strength, deformability, failure behavior and acoustic emission locations of red sandstone under triaxial compression. *Rock Mech Rock Eng* 45(4):583–606

39. Yang S-Q, Ju Y, Gao F, Gui Y-L (2016) Strength, deformability and X-ray micro-CT observations of deeply buried marble under different confining pressures. *Rock Mech Rock Eng* 49(11):4227–4244
40. Yang SQ, Yin PF, Huang YH, Cheng JL (2019) Strength, deformability and X-ray micro-CT observations of transversely isotropic composite rock under different confining pressures. *Eng Fract Mech* 214:1–20
41. You W, Dai F, Liu Y, Du H, Jiang R (2021) Investigation of the influence of intermediate principal stress on the dynamic responses of rocks subjected to true triaxial stress state. *Int J Min Sci Technol* 31(5):913–926
42. Zhang JC, Xu WY, Wang HL, Wang RB, Meng QX, Du SW (2016) A coupled elastoplastic damage model for brittle rocks and its application in modelling underground excavation. *Int J Rock Mech Min Sci* 84:130–141
43. Zhao LY, Shao JF, Zhu QZ (2018) Analysis of localized cracking in quasi-brittle materials with a micro-mechanics based friction-damage approach. *J Mech Phys Solids* 119:163–187
44. Zhao L-Y, Zhu Q-Z, Shao J-F (2018) A micro-mechanics based plastic damage model for quasi-brittle materials under a large range of compressive stress. *Int J Plast* 100:156–176
45. Zhou S-W, Xia C-C (2019) Propagation and coalescence of quasi-static cracks in Brazilian disks: an insight from a phase field model. *Acta Geotechnica* 14(4):1195–1214
46. Zhu C, Arson C (2014) A thermo-mechanical damage model for rock stiffness during anisotropic crack opening and closure. *Acta Geotechnica* 9(5):847–867

Publisher's Note Springer Nature remains neutral with regard to jurisdictional claims in published maps and institutional affiliations.

Springer Nature or its licensor holds exclusive rights to this article under a publishing agreement with the author(s) or other rightsholder(s); author self-archiving of the accepted manuscript version of this article is solely governed by the terms of such publishing agreement and applicable law.